Sustainable Marine Structures
https://journals.nasspublishing.com/index.php/sms

ARTICLE

Simulation of Longitudinal Bulkheads on Very Large Crude Carrier Hull Cross-Sections and Their Effect on Ultimate Strength

Muhammad Zubair Muis Alie [1*] , ***Sri Winda*** [1], ***Andi Mursid Nugraha Arifuddin*** [2], ***Fredhi Agung Prasetyo*** [3], ***Sukron Makmun*** [3]

[1] *Department of Ocean Engineering, Engineering Faculty, Hasanuddin University, Makassar 92171, Indonesia*
[2] *Department of Naval Architecture, Institut Teknologi Kalimantan, Balikpapan 76115, Indonesia*
[3] *Research & Development Division, PT. Biro Klasifikasi Indonesia (Persero), Jakarta 14320, Indonesia*

ABSTRACT

A bulkhead is very useful for dividing the cargo hold into some compartments and strengthening the ultimate strength, especially in the longitudinal direction. Bulkheads greatly improve structural integrity, improve damage stability by reducing flooding, and lessen the free surface effect of liquid cargoes. Longitudinal bulkheads are essential structural elements in ships, especially for big vessels such as tankers and so on. The main function of a longitudinal bulkhead, which is a vertical partition that runs the length of a ship (fore and aft), is to greatly enhance the structural integrity and safety of the vessel through compartmentalization. In larger vessels like tankers and cargo ships, they are particularly important. The additional bulkhead makes it more potent for longitudinal strength. The objective of this study is to analyze the ultimate strength of ship construction by considering the bulkhead effect. A very large crude carrier (VLCC) is the target of the object to be analyzed. The existing condition of VLCC is used as the basis for the analysis. The VLCC's cross-section is assumed to stay flat throughout the progressive collapse. The numerical analysis is adopted and implemented into the Finite Element Method to analyze the ultimate strength of the VLCC under hogging and sagging conditions. The application of Multiple Point Constraint (MPC) is performed on the VLCC cross-section model. The material properties like density, Young's modulus, yield

*CORRESPONDING AUTHOR:
Muhammad Zubair Muis Alie, Department of Ocean Engineering, Engineering Faculty, Hasanuddin University, Makassar 92171, Indonesia; Email: zubair.m@eng.unhas.ac.id

ARTICLE INFO
Received: 14 January 2026 | Revised: 11 May 2026 | Accepted: 30 June 2026 | Published Online: 7 July 2026
DOI: https://doi.org/10.36956/sms.v8i3.3084

CITATION
Muis Alie, M.Z., Winda, S., Arifuddin, A.M.N., et al., 2026. Simulation of Longitudinal Bulkheads on Very Large Crude Carrier Hull Cross-Sections and Their Effect on Ultimate Strength. Sustainable Marine Structures. 8(3): 18–32. DOI: https://doi.org/10.36956/sms.v8i3.3084

strength and Poisson's ratio are included in the model. The comparison of the ultimate strength in terms of the moment-rotation relationship is introduced in this study.

Keywords: Very Large Crude Carrier; Cross Section; Bulkhead Simulation; Ultimate Strength

1. Introduction

Bulkheads not only divide the ship into several cargo spaces but also increase the ship's strength both transversely and longitudinally. The set distance and the required amount determine the location of this bulkhead. Installing bulkheads certainly impacts the volume of cargo space on the ship. On the other hand, with the bulkhead, the ship becomes stronger. In addition, especially for tankers with bulkheads, the movement of liquids in the cargo hold can be reduced. The analysis of the ultimate strength of a ship's hull has been done using numerical or analytical methods in many studies. Rakowski and Guminiak[1] employed a computational technique implemented in finite elements to investigate the free vibrations of geometrically nonlinear elastic Timoshenko beams with fixed supports. Li and Chen[2] focused on developing empirical methods for hull structure design and safety estimation, evaluating plates under biaxial compression using nonlinear finite element analysis. Quispe et al.[3] used computational modeling and experimental methods to test a reduced-scale hull box girder for four-point bending. Deng et al.[4] investigated the ultimate strength and buckling failure behavior of single-hull and double-hull girders with wide deck apertures under cyclic ultimate bending moments using both experimental methods and finite element analysis.

To replicate the buckling/plastic collapse behavior of a real cruise ship, Shi and Gao[5] conducted a collapse experiment using a steel model with superstructures. The results of the experiment validated key elements that were included in the nonlinear finite element model, such as starting defects and welding residual stress. A Bayesian technique for probabilistic modeling was introduced by Georgiadis et al.[6] and can be used to design and evaluate cargo ships. Jagite et al.[7] investigated the dynamic maximum load-bearing capability of ultra-large container ships under actual loading conditions. Their study focused on evaluating the hull girder under lateral and localized loads caused by different cargo loading circumstances, in addition to a composite bending moment obtained from hydro-elastic research over an extended period of time. Babazadeh and Khedmati[8] built on previous research by investigating how fractures affect the ultimate longitudinal strength of a ship's hull girder. They performed a progressive collapse analysis to determine the ultimate strength of an ISSC2000 bulk carrier, taking into account crack damage at many hull girder locations, including the deck, sides, bottom, and double bottom. A finite element study of a special channel beam with thin walls and reinforced webs was carried out by Grenda and Paczos[9]. For box-shaped steel structures subjected to internal blast loading with dimensional analysis, Cong et al.[10] proposed a modified scaling method that incorporates the strain-rate effect into the material's constitutive model and develops a set of scaling conditions distinct from the conventional scaling laws.

Yuan et al.[11] addressed the limitation of previous studies by ignoring interior hull components and highlighted the study gap on the cumulative damage effect caused by multiple underwater explosions on hull structures. The precise conversion of dynamic behavior between scaled models and prototypes was supported methodologically and theoretically by Yin et al.[12]. Shi et al.[13] used model experiments with a drop-hammer facility to examine the nonlinear bending behavior of box girders under impact loads. The ultimate load-bearing capability of pre-cracked stiffened panels under the combined impacts of accumulative plasticity and low-cycle fatigue was examined by Geng and Qin[14]. The collapse behavior of a scaled, ring-stiffened HY-80 cylinder was examined by Park et al.[15]. Ma et al.[16] focused on the impact of coupled bending moments and lateral pressure on the load-bearing characteristics and failure behaviors of hull girders at different scaling factors. A geometrical distortion solution for the box-girder similarity design under longitudinal compression load was pro-

posed by Wang et al.[17]. In order to study the behaviors of wave-induced loads of a 21000TEU super large container ship, Yu et al.[18] devised a hydroelastic computational technique that predicts springing reactions by integrating a finite volume flow solver with a multibody dynamics framework. The technique, known as the "buckling strength driven similarity method, was created by Wang et al.[19] and used to hull girders under combined bending-torsion loads.

A double-hull tanker under biaxial bending was examined by Kuznecovs et al.[20] in four scenarios: an intact hull, a hull damaged in a collision, a newly constructed hull, and a corroded hull. The accuracy and processing needs of two different methods were assessed in the study. The study by Vu Van et al.[21] sought to determine how the maximum bending moment in two bulk carriers of varying sizes and types was impacted by varying corrosion levels and initial flaws. The ultimate hull girder strength of tankers and bulk carriers was analyzed using a semi-analytical approach by Muis Alie et al.[22] taking into account the effect of side hopper angle on two ships and the cross section was considered for simple calculation. Oterkus et al.[23] used the commercial program ANSYS APDL to study the container ship under hydrostatic pressure using the Finite Element Method. In order to convert the excitation force point and line transmission into surface transmission, Qin et al.[24] suggested a foundation impedance-balanced approach that replaces the conventional foundation support structure with a vibration isolation liquid layer.

Using a numerical approach, this study investigates the influence of longitudinal bulkheads on the ultimate strength of ship hull girders for VLCC. The analysis considers that progressive collapse occurs under hogging and sagging phases. The impact of the bulkhead on the ultimate strength of VLCC is a novel topic covered in the study.

2. Materials and Methods

2.1. Materials

This research examines how bulkhead location affects the ultimate strength through numerical techniques. The study examines the cross-section of VLCC hull constructions, analyzing them under conditions of hogging and sagging. The simulation of the bulkhead location is done in three stages. The first stage is the existing condition, where the location of the bulkhead does not change from the original position. In the second stage of simulation, the longitudinal bulkhead is placed in the middle of the VLCC ship's cross-section. The last stage is where one bulkhead is placed on the center line of the VLCC cross-section. The ship measures 42 m in width and 20.3 m in depth. Along the longitudinal direction, the frame spacing is fixed at 4.67 m. The ship has the same material characteristics: density, yield strength, Poisson's ratio, and Young's modulus (see **Table 1**). It is assumed that the cross-section remains planar during the assessment of progressive collapse. The analysis excludes considerations of initial deflection, corrosion, or cracks. The ultimate strength assessment of VLCC is performed under conditions of hogging and sagging. The cross-section of a VLCC is illustrated in **Figure 1**.

Table 1. Material properties.

Parameters	Value	Unit
Density	7.89×10^{-9}	N/mm^3
Young Modulus	206000	N/mm^2
Poisson Ratio	0.3	-
Yield Strength	315/355	N/mm^2

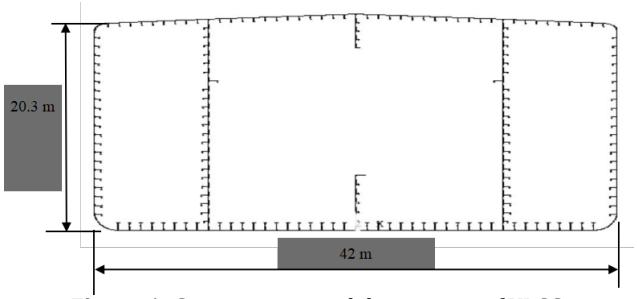

Figure 1. Cross-section and dimensions of VLCC.

2.2. Numerical Method

In this study, the models of the VLCC with simulated bulkheads are shown in **Figures 2–4**, respectively. For the model of VLCC with one bulkhead on the centerline (**Figure 3**) and the VLCC model with two symmetrical bulkheads (**Figure 4**), the plates and unstiffened plates

from the existing model are removed. In **Figure 2** (existing condition), the reinforced plate installed in the center of the ship's cross-section is not connected from bottom to top, so it is not a longitudinal bulkhead. Next, simulations are carried out in **Figures 3** and **4**. In **Figure 3**, the longitudinal bulkhead is placed in the center, while the two longitudinal bulkheads on the left and right sides are removed. In **Figure 4**, the longitudinal bulkhead is only found on the left and right sides. The size of the bulkhead varies depending on the length of the ship and its thickness also depends on the height of the ship. The rectangular shell-type Finite Element Model is imposed on a cross-section of a VLCC. Plate thickness and stiffener detail are summarized in **Tables 2** and **3**.

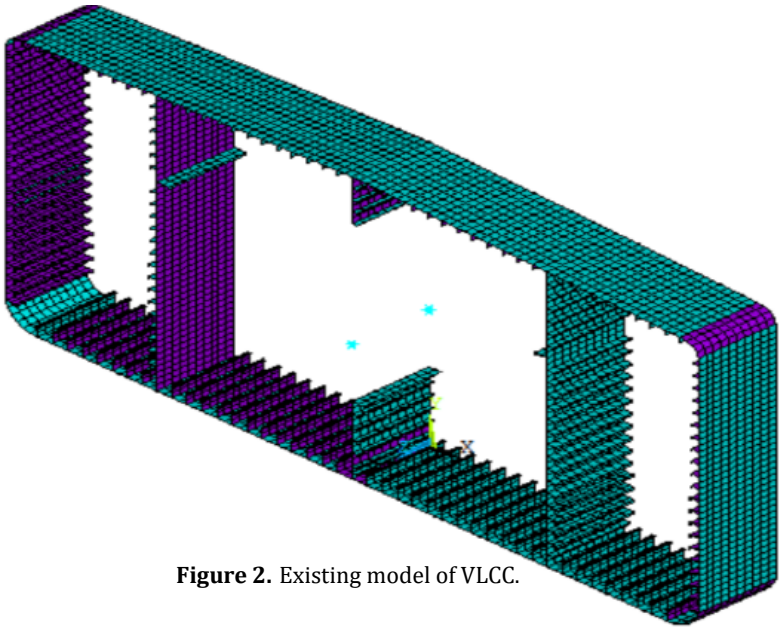

Figure 2. Existing model of VLCC.

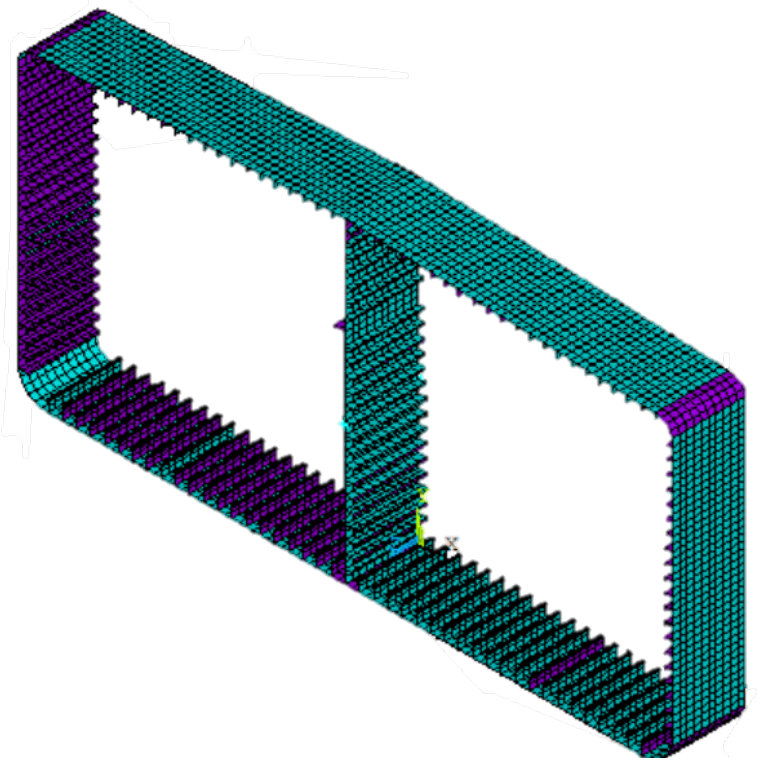

Figure 3. Model of VLCC with one bulkhead in the center line.

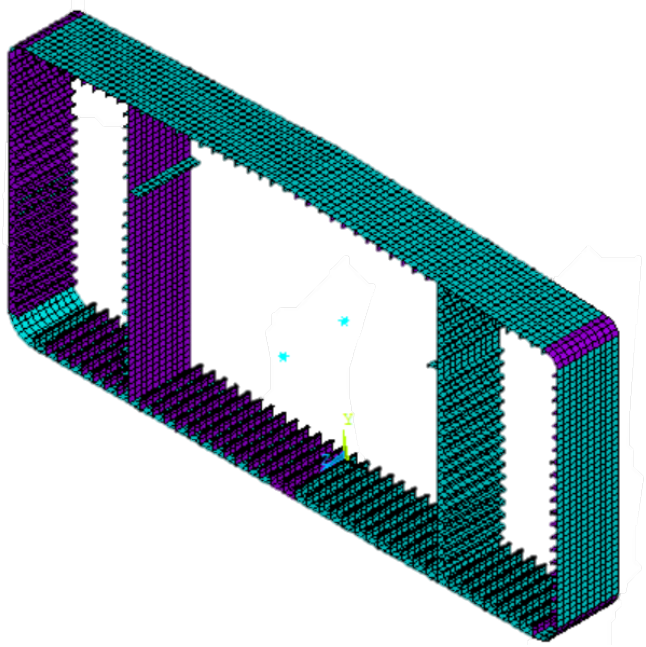

Figure 4. Model of VLCC with two symmetrical bulkheads.

Table 2. Plate thickness.

No.	Plate Thickness (mm)	No.	Plate Thickness (mm)	No.	Plate Thickness (mm)
1	14	37	18	73	24.5
2	14	38	18	74	24.5
3	14	39	18	75	24.5
4	14	40	18	76	24.5
5	14	41	18	77	24.5
6	20	42	18	78	24.5
7	20	43	18	79	24.5
8	20	44	18	80	24.5
9	20	45	18	81	18.5
10	20	46	18	82	18.5
11	20	47	18	83	18.5
12	20	48	18	84	18.5
13	23.5	49	18	85	12.5
14	23.5	50	18	86	12.5
15	22	51	18	87	12.5
16	22	52	18	88	12.5
17	22	53	18	89	12.5
18	22	54	18	90	12.5
19	22	55	18	91	12.5
20	22	56	18	92	14
21	22	57	24.5	93	14
22	22	58	24.5	94	14
23	22	59	24.5	95	14
24	22	60	24.5	96	15
25	22	61	24.5	97	15
26	22	62	24.5	98	15
27	22	63	24.5	99	15
28	22	64	24.5	100	16
29	22	65	24.5	101	16
30	22	66	24.5	102	16
31	22	67	24.5	103	18.5
32	22	68	24.5	104	18.5
33	22	69	24.5	105	18.5
34	22	70	24.5	106	22
35	22	71	24.5	107	24.5
36	18	72	24.5	108	24.5

Table 3. Stiffener detail.

No.	Web Height (mm)	Web Thickness (mm)	Flange Breadth (mm)	Flange Thickness (mm)	Type
1	250	12	67	18	Angle-Bar
2	250	12	67	18	Angle-Bar
3	250	12	67	18	Angle-Bar
4	300	12	-	-	Flat-Bar
5	700	12	-	-	Flat-Bar
6	250	12	67	18	Angle-Bar
7	250	12	67	18	Angle-Bar
8	250	12	67	18	Angle-Bar
9	250	12	67	18	Angle-Bar
10	250	12	67	18	Angle-Bar
11	675	13	200	25	Tee-Bar
12	675	13	200	25	Tee-Bar
13	675	13	200	25	Tee-Bar
14	675	13	200	25	Tee-Bar
15	675	13	200	25	Tee-Bar
16	675	13	200	25	Tee-Bar
17	675	13	200	25	Tee-Bar
18	675	13	200	25	Tee-Bar
19	675	13	200	25	Tee-Bar
21	675	13	200	25	Tee-Bar
22	675	13	200	25	Tee-Bar
23	675	13	200	25	Tee-Bar
24	675	13	200	25	Tee-Bar
25	675	13	200	25	Tee-Bar
26	675	13	200	25	Tee-Bar
27	675	13	200	25	Tee-Bar
28	675	13	200	25	Tee-Bar
29	675	13	200	25	Tee-Bar
30	675	13	200	25	Tee-Bar
31	572	12	150	22	Angle-Bar
32	572	12	150	22	Angle-Bar
33	572	12	150	22	Angle-Bar
35	522	11	150	22	Angle-Bar
36	522	11	150	22	Angle-Bar
37	518	11.5	150	18	Angle-Bar
38	518	11.5	150	18	Angle-Bar
39	518	11.5	150	18	Angle-Bar
40	518	11.5	150	18	Angle-Bar
41	468	11.5	125	18	Angle-Bar
42	468	11.5	125	18	Angle-Bar
43	468	11.5	125	18	Angle-Bar
44	468	11.5	125	18	Angle-Bar
45	400	12	100	18	Angle-Bar
46	400	12	100	18	Angle-Bar
47	350	12	100	17	Angle-Bar
48	350	12	100	17	Angle-Bar
49	350	12	100	17	Angle-Bar
50	350	12	100	17	Angle-Bar
51	350	12	100	17	Angle-Bar
52	350	28	-	-	Flat-Bar
53	350	28	-	-	Flat-Bar
54	350	28	-	-	Flat-Bar
55	350	28	-	-	Flat-Bar
56	350	28	-	-	Flat-Bar
58	350	28	-	-	Flat-Bar
59	350	28	-	-	Flat-Bar
60	350	28	-	-	Flat-Bar
61	350	28	-	-	Flat-Bar
62	350	28	-	-	Flat-Bar
63	350	28	-	-	Flat-Bar
64	350	28	-	-	Flat-Bar
65	350	28	-	-	Flat-Bar
66	350	28	-	-	Flat-Bar
67	350	28	-	-	Flat-Bar
68	350	28	-	-	Flat-Bar

Table 3. *Cont.*

No.	Web Height (mm)	Web Thickness (mm)	Flange Breadth (mm)	Flange Thickness (mm)	Type
69	350	28	-	-	Flat-Bar
71	350	28	-	-	Flat-Bar
72	350	28	-	-	Flat-Bar
73	350	12	100	17	Angle-Bar
74	350	12	100	17	Angle-Bar
75	350	12	100	17	Angle-Bar
76	350	12	100	17	Angle-Bar
77	350	12	100	17	Angle-Bar
78	350	12	100	17	Angle-Bar
79	716	12.5	150	16	Angle-Bar
80	400	12	125	18	Angle-Bar
81	400	12	125	18	Angle-Bar
82	450	11.5	125	18	Angle-Bar
83	450	11.5	125	18	Angle-Bar
84	450	11.5	125	18	Angle-Bar
85	450	11.5	125	18	Angle-Bar
86	500	11.5	150	18	Angle-Bar
87	500	11.5	150	18	Angle-Bar
88	500	11.5	150	18	Angle-Bar
89	500	11.5	150	18	Angle-Bar
90	500	11.5	150	18	Angle-Bar
91	522	11	150	22	Angle-Bar
92	572	12	150	22	Angle-Bar
93	572	12	150	22	Angle-Bar
95	350	12	100	17	Angle-Bar

The Multiple Point Constraint (MPC) method is applied using the neutral axis position as the reference point. The neutral position, area, inertia, and section modulus are 8,838 mm, 1,267,200 mm^2, 6.43 × 10^{18} mm^4, 7.4 × 10^{18} mm^3, respectively. The ultimate strength analysis of a VLCC uses the Finite Element Method in ANSYS. The cross-section is subjected to a rotational force while ensuring it remains plane throughout the progressive collapse analysis. One side of the cross-section is restrained, and the other side is subjected to the rotational force. The load and boundary conditions are illustrated in **Figure 5**. The element type is a shell element, and the mesh size used in the model is 300 mm. The model material used is elastic-plastic with isotropic hardening. The convergence criteria, such as force, displacement, and energy, are also checked for the analysis running. Nonlinear analysis was performed with material nonlinearity to capture steel yielding and strain hardening, and geometric nonlinearity NLGEOM = ON to account for large displacement and post-buckling behavior. The Riks arc-length method was used with displacement control to trace the post-ultimate strength path.

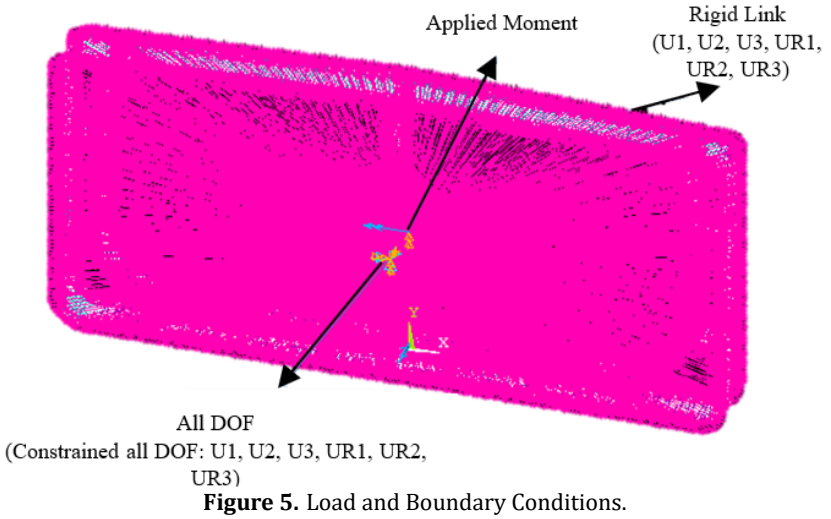

Figure 5. Load and Boundary Conditions.

2.3. Analytical Method

It is commonly acknowledged in practice that the simple beam theory is one method for analyzing the progressive collapse behavior of a ship hull girder subjected to longitudinal bending. Muis Alie [25] also utilized this approach to confirm that a ship's bending behavior closely follows beam theory. The cross-section of the ship serves as a representation of the bending strength of the main hull structure, emphasizing the significance of hull girder cross-section calculation in ship design. This calculation considers structural elements that extend along the longitudinal direction. These parts, including the associated plating, are classified as stiffeners and plates. Thin-walled beam theory is the foundation of the Beam-Element formulation. The coordinate system is formed by the z-axis running down perpendicular to the length of the beam and the x- and y-axes lying inside the beam's cross-section. The centroid of the cross-section serves as the coordinate system's origin, and the mid-thickness line is where the s-coordinate is measured. The displacements U, V, and W in the x, y, and z directions at the coordinate (x, y, z) may be written in Equations (1)–(3) as follows, assuming that the cross-section remains plane during deformation.

$$U(x,y,z) = u_s(z) - (y - y_s)\,\theta(z) \tag{1}$$

$$V(x,y,z) = \nu_s(z) + (x - x_s)\,\theta(z) \tag{2}$$

$$W(x,y,z) = w(z) - xu_s^{'}(z) - yv_s^{'}(z) + \omega_{ns}(x,y)\theta^{'}(z) \tag{3}$$

u_s and v_s stand for the displacements in the x- and y-axis directions, respectively, at the shear center. While w shows the displacement along the z-axis at the gravity center. The symbol, represents the rotation angle about the shear center θ. The x_s andy_s are the x and y coordinates of the shear center. ω_{ns} shows the warping function concerning the center of the shear. Differentiation concerning the z-coordinate is indicated by a prime ('). Equations (1) and (2) yield stresses derived from displacements, which may be represented in Equations (4) and (5).

$$\varepsilon_z = w^{'} - xu_s^{''} - yv_s^{''} + \omega_{ns}\theta^{''} \tag{4}$$

$$\gamma_{sz} = \gamma_{xz}\frac{\partial x}{\partial s} + \gamma_{yz}\frac{\partial y}{\partial s} = \left\{\frac{\partial \omega_{ns}}{\partial s} - (y - y_s)\frac{\partial x}{\partial s} + (x - x_s)\frac{\partial y}{\partial s}\right\}\theta^{'} \tag{5}$$

ε_z describes the strain in the z-axis direction. γ_{sz} shows shear strain in the s-z plane. The relationship between stress and strain can be expressed as Equation (6).

$$\begin{pmatrix}\sigma_z \\ \tau_{sz}\end{pmatrix} = \begin{bmatrix} d_{11} & d_{12} \\ d_{21} & d_{22}\end{bmatrix}\begin{pmatrix}\varepsilon_z \\ \gamma_{sz}\end{pmatrix} \tag{6}$$

The axial stress is given by σ_z, while the shear stress in the s-z plane is represented by τ_{sz}, the term d_{ij} describes the stress-strain relationship. The stiffness of segmented components, including both plates and stiffened plates, is represented by d_{ij}. In this study, the ship's cross-section is modeled as a thin-walled beam, which is affected by yielding and buckling. The finite element approach uses a beam element between nodes *ij*, which is further split along the z-direction. The symbol for this element's length is l. The nodal displacement at the shear center is represented by the vector {u_s}, which includes translation along the x-axis and its derivative concerning z (shown by '). Node *i* is indicated here by the subscript *i*. Likewise, the displacements at additional nodes can be shown as in Equations (7)–(11).

$$\{u_s\}^T = \left[u_{si}\ ,\ u_{si}^{'},\ u_{sj},\ u_{sj}^{'}\right] \tag{7}$$

$$\{v_s\}^T = \left[v_{si}\ ,\ v_{si}^{'},\ v_{sj},\ v_{sj}^{'}\right] \tag{8}$$

$$\{\theta_s\}^T = \left[\theta_i\ ,\ \theta_i^{'},\ \theta_j,\ \theta_j^{'}\right] \tag{9}$$

$$\{w\}^T = [w_i\ ,\ w_j\ ] \tag{10}$$

$$\{d\}^T = \left[\{u_s\}\ ,\ \{v_s\}\ ,\ \{\theta\},\ \{w\}\right] \tag{11}$$

The displacement vector of nodes in the y-direction at the shear center is represented as $\{v_s\}$, The torsion angle relative to the shear center and the rate of torsion are expressed as $\{\theta\}$, the axial displacement at the center of gravity is represented as $\{w\}$. In the same way, the nodal forces are specified as Equations (12)–(16).

$$\{F_u\}^T = \left[F_{xi}\ ,\ M_{yi}\ ,\ F_{xj},\ M_{yj}\right] \tag{12}$$

$$\{F_v\}^T = \left[F_{yi}\ ,\ M_{xi}\ ,\ F_{yj},\ M_{xj}\right] \tag{13}$$

$$\{F_\theta\}^T = \left[T_i\ ,\ B_i\ ,\ T_j,\ B_j\right] \tag{14}$$

$$\{F_w\}^T = [F_{zi}\ ,\ F_{zj}\ ] \tag{15}$$

$$\{F\}^T = \left[\{F_u\}\ ,\ \{F_v\}\ ,\ \{F_\theta\},\ \{F_w\}\right] \tag{16}$$

The shear forces and bending moments are denoted by $\{F_u\}$and $\{F_v\}$, the torsional and bi-moment around the axis at the shear center are denoted by $\{F_\theta\}$, and $\{F_w\}$ represents the axial force. As interpolated linearly for the axial displacement $w(z)$ within the element and cubic polynomials for the horizontal and vertical deflections $u_s(z)$, $v_s(z)$ and torsion angle $\theta(z)$. The following form may represent the displacement functions as a function of the nodal displacements using the coordinates and nodal displacements.

$$u_s(z) = [A_c(z)]\{u_s\} \; ; \; v_s(z) = [A_c(z)]\{v_s\}$$
$$\theta(z) = [A_c(z)]\{\theta\} \; ; \; w(z) = [A_L(z)]\{w\}$$

where

$$[A_c(z)] = \begin{bmatrix} 1 & z & z^2 & z^3 \end{bmatrix} \begin{bmatrix} 1 & 0 & 0 & 0 \\ 0 & 1 & 0 & 0 \\ \frac{-3}{l^2} & \frac{2}{l} & \frac{3}{l^2} & \frac{2}{l} \\ \frac{2}{l^3} & \frac{1}{l^2} & \frac{-2}{l^3} & \frac{1}{l^2} \end{bmatrix};$$
$$[A_L(z)] = \begin{bmatrix} 1 & z \end{bmatrix} \begin{bmatrix} 1 & 0 \\ \frac{-1}{2} & \frac{1}{2} \end{bmatrix} \quad (17)$$

The axial and shear stresses can be represented by substituting Equation (17) into Equations (4) and (5), yielding Equation (18):

$$\begin{pmatrix} \varepsilon_z \\ \gamma_{sz} \end{pmatrix} = \begin{bmatrix} [B_1] & -x[B_2] & -y[B_3] & \omega_{ns}[B_2] \\ 0 & 0 & 0 & g(s)[B_3] \end{bmatrix} \{d\}$$

where

$$[B_1] = \frac{d}{d_z}[A_L] \; , \; [B_2] = \frac{d^2}{d_z^2}[A_C] \; ,$$
$$[B_3] = \frac{d}{d_z}[A_C] \; , \; g(s) = \frac{\partial \omega_{ns}}{\partial_s} - (y - y_s)\frac{\partial x}{\partial s} + (x - x_s)\frac{\partial y}{\partial s} \quad (18)$$

The incremental version of the stiffness equation is obtained by applying the principle of virtual work with the stress and strain increments, which yields Equation (19).

$$\{\Delta F\} = [K]\{\Delta d\} \quad (19)$$

where $[K]$ provides the stiffness formula in Equation (20).

$$[K] = \int_V \begin{bmatrix} d_{11}[B_1] & -xd_{11}[B_{12}] & -yd_{11}[B_{12}] & \omega_{ns}d_{11}[B_{12}] \\ -xd_{11}[B_{21}] & x^2 d_{11}[B_2] & xyd_{11}[B_2] & -x\omega_{ns}d_{11}[B_2] \\ -yd_{11}[B_{21}] & xyd_{11}[B_2] & y^2 d_{11}[B_2] & -y\omega_{ns}d_{11}[B_2] \\ \omega d_{11}[B_{21}] & -x\omega_{ns}d_{11}[B_2] & -y\omega_{ns}d_{11}[B_2] & \omega_{ns}^2 d_{11}[B_2] + g^2 d_{22}[B_3] \end{bmatrix} \quad (20)$$

According to Equation (6), the stress-strain relationship at any location for an elastic cross-section with constant material characteristics is $d_{11} = E$, $d_{22} = G$, $d_{12} = d_{21} = 0$ where *E* and *G* denote the Young's modulus and shear modulus, respectively.

3. Results and Discussions

3.1. Hull Girder Loads

The various loads acting on the ship structure are static and dynamic. The static loads could be the weight of the ship and the dynamic loads produced by waves, currents, and wind. For the design and analysis of ship structure, static and dynamic loads are the most common to be considered. The components of the hull girder loads are vertical bending, horizontal bending, shear, and torsional moment, as illustrated in **Figures 6** and **7** by Hughes and Paik[26].

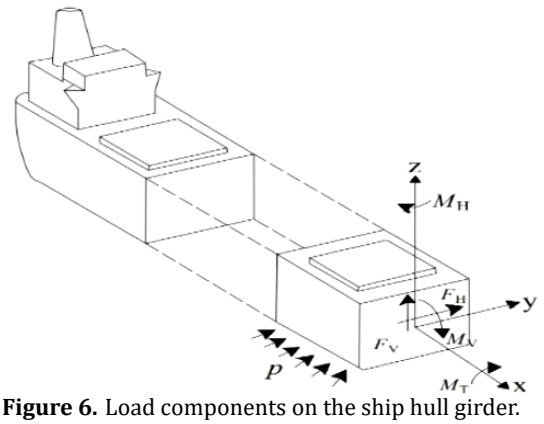

Figure 6. Load components on the ship hull girder.

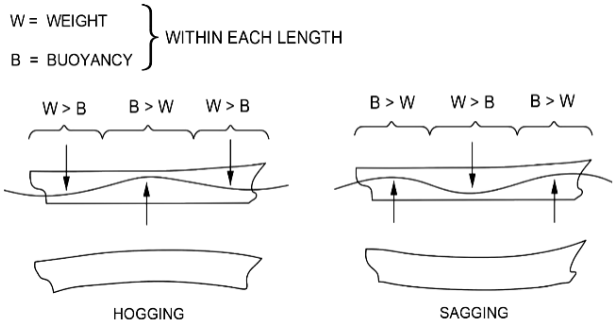

Figure 7. Hogging and sagging load components.

The total vertical bending moment M_t can be obtained by the summation of the still water bending moment M_{SW} and wave-induced bending moment M_W as written in Equation (21). Under pure vertical bending, the following condition must be satisfied where the axial stress over the area of the ship cross-section is equal to zero, as described in Equation (22).

$$M_t = M_{SW} + M_W \tag{21}$$

$$\int \sigma \, dA = 0 \tag{22}$$

From here, the stress that occurs in the deck part, bottom part, and bending moments, including its deformation, can be obtained since the neutral axis position has been determined in advance.

3.2. Ultimate Strength

In the present study, the ultimate strength of VLCC is determined using numerical methods. The ultimate strength of VLCC is obtained in terms of the moment-rotation curve or moment-curvature relationship for the moment-rotation relationships for three models, namely existing, one center bulkhead, and two side bulkheads. The three models are shown in **Figures 8–10**, respectively. The ultimate strength of a ship hull girder under hogging and sagging conditions could be read from the moment-curvature or moment-rotation relationship, as demonstrated in studies by Ma et al.[16], Quispe et al.[3], and Zhao et al.[27]. **Figures 8–10** compare the ultimate strength of three VLCC models using the numerical and beam element approaches. The solid line represents the moment-rotation relationships obtained through the numerical method, while the dashed line indicates the strength calculated using the beam element approach. The numerical method generally yields a higher ultimate strength than the beam element approach, likely due to the localized stress distribution within the elements. The bending stiffness of the three models varies due to bulkheads positioned at the center and on both sides of the VLCC cross-section.

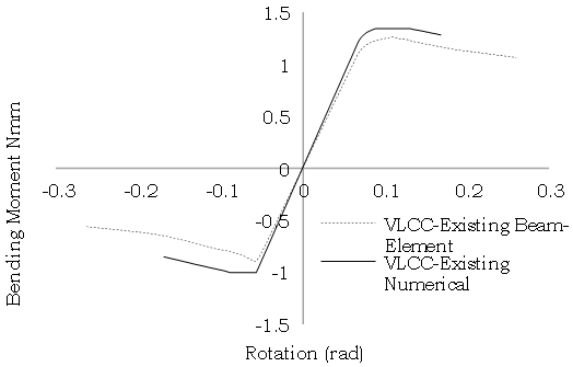

Figure 8. Comparison of the moment-rotation of the existing condition.

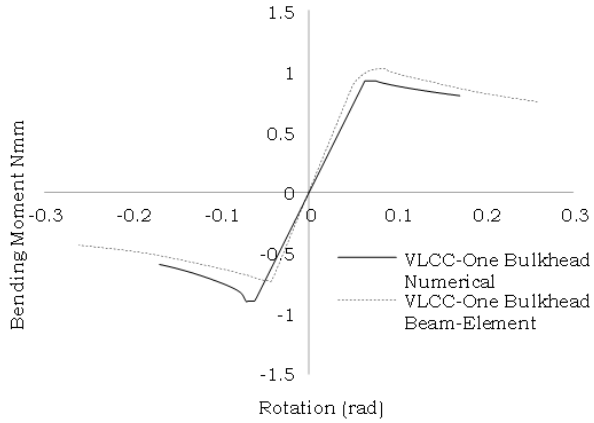

Figure 9. Comparison of the moment-rotation of one center bulkhead.

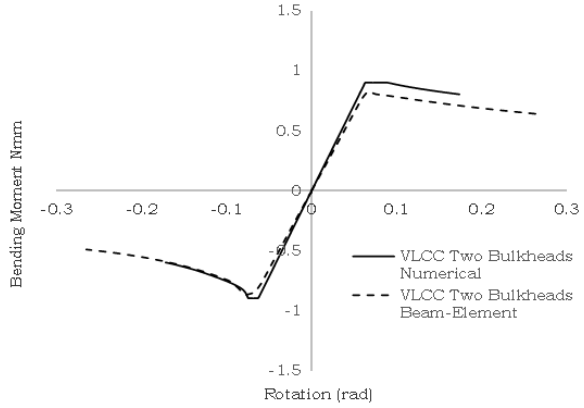

Figure 10. Comparison of the moment-rotation of two side bulkheads.

A hull girder sagging or hogging is mechanically similar to a massive I-beam. The side shell and longitudinal bulkheads serve as the web, and the deck and bottom plates serve as the top and bottom flanges. Hull girder collapse usually starts with the deck buckling under compression during sagging if there are no longitudinal bulkheads. As a result, the deck as a whole dented downward like a single, broad panel. The collapse mode shifts to a "progressive collapse" panel per panel when longitudinal bulkheads are present. The highest bending moment capacity that the ship's cross-section can sustain before global failure happens is the longitudinal hull girder's ultimate strength. The longitudinal bulkhead of contemporary tankers, bulk carriers, and LNG carriers not only acts as a cargo separator but also makes a substantial contribution to the longitudinal bending strength and stiffness. Longitudinal bulkheads also increase torsional stiffness. Warping stress, which causes deck cracking at opening corners is reduced. Even when the ship is subjected to pure bending, the torsional effects cannot be ignored because longitudinal bulkheads also function as "closed sections" that block shear flow. Longitudinal bulkheads are not only the number that influences the longitudinal strength of the ship, but the position of the bulkheads is also critical. Furthermore, the factors that modify the effect of bulkheads and their contribution to ship strength include: bulkhead-to-deck thickness ratio, bulkhead-deck-bottom connectivity, the presence of large openings, lateral loads, and material grade.

Table 4 shows the ultimate strength results for both methods under hogging and sagging conditions. The difference in ultimate strength between the numerical method and beam element on VLCC for the existing one bulkhead in the middle and two bulkheads on the left and right sides under hogging conditions is 6.7%, 8.8%, and 9.8%, respectively. Meanwhile, in sagging conditions, the difference in ultimate strength between the numerical method and beam elements on existing VLCC vessels, one bulkhead in the middle and two bulkheads on the sides, is 11%, 15.9%, and 2.6%. The percentage result of the ultimate strength obtained by the numerical method and by using beam elements indicates that the additional bulkhead influences the ultimate strength. The VLCC tanker analyzed in this study is a single-hull tanker. In this case, the inner bottom plates on the bottom, port and starboard sides of the ship are not installed. Therefore, bulkheads are crucial to the ship's ultimate longitudinal strength. In the present model, the bulkheads are symmetrically located on the left and right sides, with a stiffener plate at the center (centerline) of the ship's cross-section. This stiffener plate contributes to the ship's longitudinal strength. In the second simulation model, the bulkheads are only installed in the center, so that under bending conditions, only the bulkhead in the center supports the longitudinal strength of the structure, while the port and starboard sides do not. Meanwhile, in the third simulation model, the bulkheads are symmetrically located on the left and right sides, but there is no panel in the center as in the existing (present) model. Therefore, under bending conditions, only the left and right sides support the longitudinal strength, while the center section does not. The ultimate strength in the existing condition is higher than that of two bulkheads and one bulkhead. This is because the existing condition has elements on the centerline of the VLCC's cross-section.

Table 4. Ultimate Bending Moment.

Condition	Method	Ultimate Hogging Moment × 10^{12} (Nmm)	Ultimate Sagging Moment × 10^{12} (Nmm)
Existing	Numerical	1.35	−1.00
	Beam Element	1.26	−0.89
One center bulkhead	Numerical	0.93	−0.88
	Beam Element	1.02	−0.74
Two side bulkheads	Numerical	0.92	−0.89
	Beam Element	0.83	−0.867

Regarding the comparison of single-hull and double-hull VLCC vessels, the double-hull configuration of VLCC ships increases the hull bearing moment of inertia due to the relocation of the side structure mate-

rial further from the neutral axis and the presence of wing bulkheads. As a result, the bending stiffness (EI) increases proportionally, reducing the hull bearing deflection at the same bending moment. This higher stiffness also leads to a higher ultimate bending moment, as the deck section buckles. However, the increase in steel weight is relatively small, making the double hull structurally more efficient in terms of EI/ton. Double-hull VLCC vessels are 50% stiffer than single-hull ships due to the geometry, such as the box and longitudinal bulkheads. Deflections and stresses are reduced; on the other hand, bending moments increase with a relatively small weight. Longitudinal bulkheads increase bending moment capacity. The mechanism is to increase cross-sectional inertia, narrow the deck panels, and provide additional shear webs. Bulkheads change the collapse mode from ”global deck buckling” to ”progressive collapse panel by panel.” Bulkhead effectiveness is highly dependent on scantling and connectivity. The number and position of longitudinal bulkheads also influence the bending stiffness. The number and position of bulkheads directly affect the bending stiffness. The more bulkheads and the greater their distance from the centerline, the greater the bending stiffness. Furthermore, this bending stiffness has a cascade effect: global deflection, stresses in the deck and bottom, natural frequencies, and asymmetric sensitivity. Longitudinal bulkheads contribute to the bending stiffness of the hull beam through the second moment of inertia (I). With the addition of the number of bulkheads on the left side or right side at a certain distance from the centerline, the moment of inertia or inertia of the cross-section will be greater compared to the configuration without bulkheads. As a result, the bending stiffness (EI) increases proportionally, resulting in a reduction in the deflection of the hull beam under the same bending moment. Its effectiveness is highly dependent on the location of the bulkheads due to the variable distance to the power of two (d^2) in the parallel axis theorem.

From a CSR perspective, longitudinal bulkheads are no longer ”optional.” For ships longer than 200 m and wider than 45 m, meeting bending moment capacity requirements without longitudinal bulkheads is nearly impossible, unless the deck is thickened to an economically disadvantageous extreme. The critical area is no longer just the deck, but the lower strake of the longitudinal bulkhead. Thus, longitudinal bulkheads should be viewed not merely as ”cargo bulkheads,” but as the primary structural element determining the ultimate strength of the hull girder. Neglecting their contribution in initial calculations will result in an understrength design. The results of this study support modern VLCC design practices and recommend that future bending moment capacity studies always model bulkheads with realistic scantling and imperfection details.

4. Conclusions

This study employs numerical analysis to assess the ultimate longitudinal strength of a VLCC ship hull girder, considering the effect of the influence of the location of the longitudinal bulkhead under both hogging and sagging conditions. The results indicate that the existing model exhibits the highest ultimate strength, followed by the configuration with two bulkheads on the left and right sides, and lastly, the setup with a single bulkhead in the middle of the ship's cross-section. The number of longitudinal bulkheads affects the ship's longitudinal strength, but their location is equally important. In this study, a single-hull VLCC tanker is examined. The bulkheads in the current model are symmetrically positioned on the left and right sides, with a stiffener plate at the ship's cross-sectional centerline. The longitudinal strength of the ship is enhanced by this stiffener plate. The bulkheads in the second simulation model are only positioned in the center, meaning that under bending conditions, only the bulkhead in the center supports the structure's longitudinal strength; the bulkheads on the left and right sides do not. The bulkheads are symmetrically positioned on the left and right sides of the third simulation model, unlike the current model, there isn't a panel in the middle. As a result, the center section does not support the longitudinal strength under bending conditions; only the left and right sides do. Compared to two bulkheads and one bulkhead, the ultimate strength under current conditions is greater. This is due to components on the centerline of the VLCC's cross-section in the current state. The bending stiffness is

also affected by the quantity and location of longitudinal bulkheads. The bending stiffness increases with the number of bulkheads and their distance from the centerline. Through the second moment of inertia (I), longitudinal bulkheads add to the hull beam's bending rigidity. The moment of inertia or inertia of the cross-section will be higher when bulkheads are added to the left or right side at a specific distance from the centerline than when bulkheads are not present. The findings highlight that the location of the bulkhead significantly impacts the ultimate strength of the ship's structure. Additionally, the numerical method results align well with those obtained using the beam element approach. The importance of this study where bulkhead position simulation is important because bulkheads directly determine panel size and load paths. Simulations provide an idea of where bulkheads should be placed to strengthen the ship's structure. Furthermore, this study is also important because it provides quantitative data for validating the method, such as Smith's method, developing a ship structure community benchmark, exploring complex interaction effects, and ensuring the reproducibility of research results in ship structural design.

Author Contributions

Writing original draft: M.Z.M.A.; Review & editing: M.Z.M.A., A.M.N.A., F.A.P., S.M., and S.W.; Visualization: M.Z.M.A. and S.W.; Validation: M.Z.M.A., A.M.N.A., and S.W.; Calculation procedure: M.Z.M.A. and S.W.; Project administration: M.Z.M.A.; Methodology: M.Z.M.A. and F.A.P.; Investigation: M.Z.M.A., F.A.P., and S.W.; Formal analysis: M.Z.M.A. and S.W.; Data curation: M.Z.M.A.; Conceptualization: M.Z.M.A., A.M.N.A., and S.M.; Supervision: A.M.N.A., F.A.P., and S.M.; Resources: A.M.N.A., F.A.P., and S.M.; Data analysis: S.W. All authors have read and agreed to the published version of the manuscript.

Funding

The research is funded by Hasanuddin University through the Professor Grants contract number 31674/UN4.1.2/HK.07.00/2024.

Institutional Review Board Statement

Not applicable.

Informed Consent Statement

Not applicable.

Data Availability Statement

The data used to support the findings of this study are included within the article.

Conflicts of Interest

The authors declare that there is no conflict of interest.

AI Use Statement

The authors use Grammarly for grammar checking, sentence structure refinement, and improving the readability of the English text. The authors also use QuillBot for sentence paraphrasing. The authors subsequently reviewed and edited the content as necessary and take full responsibility for the final content of the published article.

References

[1] Rakowski, J., Guminiak, M., 2015. Non-linear vibration of Timoshenko beams by finite element method. Journal of Theoretical and Applied Mechanics. 731. DOI: https://doi.org/10.15632/jtam-pl.53.3.731

[2] Li, D., Chen, Z., 2023. Advanced empirical formulae for the ultimate strength assessment of continuous hull plate under combined biaxial compression and lateral pressure. Engineering Structures. 285, 116041. DOI: https://doi.org/10.1016/j.engstruct.2023.116041

[3] Quispe, J.P., Estefen, S.F., Lourenço De Souza, M.I., et al., 2022. Numerical and experimental analyses of ultimate longitudinal strength of a small-scale hull box girder. Marine Structures. 85, 103273. DOI: https://doi.org/10.1016/j.marstruc.2022.103273

[4] Deng, H., Yuan, T., Gan, J., et al., 2022. Experimental and numerical investigations on the collapse behaviour of box type hull girder subjected to cyclic ultimate bending moment. Thin-Walled Structures. 175, 109204. DOI: https://doi.org/10.1016/j.tws.2022.109204

[5] Shi, G., Gao, D., 2021. Model experiment of large superstructures' influence on hull girder ultimate strength for cruise ships. Ocean Engineering. 222, 108626. DOI: https://doi.org/10.1016/j.oceaneng.2021.108626

[6] Georgiadis, D.G., Samuelides, E.S., Straub, D., 2023. A Bayesian analysis for the quantification of strength model uncertainty factor of ship structures in ultimate limit state. Marine Structures. 92, 103495. DOI: https://doi.org/10.1016/j.marstruc.2023.103495

[7] Jagite, G., Bigot, F., Malenica, S., et al., 2022. Dynamic ultimate strength of a ultra-large container ship subjected to realistic loading scenarios. Marine Structures. 84, 103197. DOI: https://doi.org/10.1016/j.marstruc.2022.103197

[8] Babazadeh, A., Khedmati, M.R., 2021. Progressive collapse analysis of a bulk carrier hull girder under longitudinal vertical bending moment considering cracking damage. Ocean Engineering. 242, 110140. DOI: https://doi.org/10.1016/j.oceaneng.2021.110140

[9] Grenda, M., Paczos, P., 2019. Experimental and numerical study of local stability of non-standard thin-walled channel beams. Journal of Theoretical and Applied Mechanics. 57(3), 549–562. DOI: https://doi.org/10.15632/jtam-pl/109601

[10] Cong, P., Wang, X., Zhou, H., 2025. Scaling the response of box-shaped steel structures subjected to internal blast loading. Structures. 80, 109908. DOI: https://doi.org/10.1016/j.istruc.2025.109908

[11] Yuan, K., Li, X., Peng, Y., et al., 2026. Cumulative damage effect of scaled hull model subjected to repeated underwater explosions. Thin-Walled Structures. 230, 115206. DOI: https://doi.org/10.1016/j.tws.2026.115206

[12] Yin, Y., Shi, D., Huang, R., et al., 2026. Nonlinear dynamic response analysis and similarity conversion method for hull model experiments based on self-similar theory. Thin-Walled Structures. 227, 115036. DOI: https://doi.org/10.1016/j.tws.2026.115036

[13] Shi, G., Wang, D., Wang, F., 2025. Experimental investigation of the critical collapse behaviour of stiffened box girders under impact bending load. Structures. 79, 109440. DOI: https://doi.org/10.1016/j.istruc.2025.109440

[14] Geng, X., Qin, D., 2025. Experimental study on ultimate bearing capacity of pre-cracked ship hull stiffened panel under low-cycle fatigue and accumulative plasticity coupling. International Journal of Naval Architecture and Ocean Engineering. 17, 100688. DOI: https://doi.org/10.1016/j.ijnaoe.2025.100688

[15] Park, S.-H., Yu, Y.-J., Cho, S.-R., et al., 2026. An experimental and numerical study on the hydrostatic collapse of a scaled HY-80 pressure hull. International Journal of Naval Architecture and Ocean Engineering. 18, 100731. DOI: https://doi.org/10.1016/j.ijnaoe.2025.100731

[16] Ma, H., Wang, Q., Wang, D., 2022. Scaling characteristics of the hull girder's ultimate strength subjected to the combined hogging moment and bottom lateral pressure: An empirically modified scaling criterion. Ocean Engineering. 257, 111520. DOI: https://doi.org/10.1016/j.oceaneng.2022.111520

[17] Wang, Z., Liu, X., Kong, X., et al., 2025. Geometrical distortion solution for the similarity design of box-girder subjected to longitudinal compression based on numerical and experimental analyses. Thin-Walled Structures. 212, 113200. DOI: https://doi.org/10.1016/j.tws.2025.113200

[18] Yu, P., Zhang, R., Guo, H., et al., 2026. Numerical simulation study on the characteristics of wave induced loads of a 21000TEU ultra-large containership. International Journal of Naval Architecture and Ocean Engineering. 18, 100756. DOI: https://doi.org/10.1016/j.ijnaoe.2026.100756

[19] Wang, Y., Zeng, Q., Wei, P., et al., 2025. Buckling strength driven similarity method for hull girders under combined loads of bending and torsion. Thin-Walled Structures. 216, 113689. DOI: https://doi.org/10.1016/j.tws.2025.113689

[20] Kuznecovs, A., Ringsberg, J.W., Johnson, E., et al., 2020. Ultimate limit state analysis of a double-hull tanker subjected to biaxial bending in intact and collision-damaged conditions. Ocean Engineering. 209, 107519. DOI: https://doi.org/10.1016/j.oceaneng.2020.107519

[21] Vu Van, T., Yang, P., Doan Van, T., 2018. Effect of uncertain factors on the hull girder ultimate vertical bending moment of bulk carriers. Ocean Engineering. 148, 161–168. DOI: https://doi.org/10.1016/j.oceaneng.2017.11.031

[22] Muis Alie, M.Z., Zakki, A.F., Setyawan, D., et al., 2026. Semi-Analytical Approach to Analyze the Hull Girder Ultimate Strength Considering the Influence of Side Hopper. International Journal of Technology. 17(1), 205–218. DOI: https://doi.org/10.14716/ijtech.v17i1.8010

[23] Oterkus, S., Wang, B., Oterkus, E., et al., 2022. Structural Integrity Analysis of Containers Lost at Sea Using Finite Element Method. Sustainable Marine

Structures. 4(2), 11–17. DOI: https://doi.org/10.36956/sms.v4i2.505

[24] Qin, Y., Wang, Y., Pang, F., et al., 2023. Vibration Isolation Characteristics of Impedance-balanced Ship Equipment Foundation under Unbalanced Excitation. Sustainable Marine Structures. 5(1), 37–47. DOI: https://doi.org/10.36956/sms.v5i1.856

[25] Muis Alie, M.Z., 2016. Residual Strength Analysisof Asymmetrically Damaged Ship Hull GirderUsing Beam Finite Element Method. Makara Journal of Technology. 20(1), 7–12. DOI: https://doi.org/10.7454/mst.v20i1.3049

[26] Hughes, O.F., Paik, J.K., 2010. Ship Structural Analysis and Design. The Society of Naval Architects and Marine Engineers: Alexandria, VA, USA.

[27] Zhao, N., Chen, B.-Q., Zhou, Y.-Q., et al., 2022. Experimental and numerical investigation on the ultimate strength of a ship hull girder model with deck openings. Marine Structures. 83, 103175. DOI: https://doi.org/10.1016/j.marstruc.2022.103175